

Article

Research on Backstepping Linear Active Disturbance Rejection Control of Hypersonic Vehicle

Chengwei Bao, Guixin Zhu * and Tong Zhao

College of Automation and Electronic Engineering, Qingdao University of Science and Technology, Qingdao 266061, China; 2022040001@mails.qust.edu.cn (C.B.); zhaotong@qust.edu.cn (T.Z.)

* Correspondence: qdzgxqust@163.com

Abstract: In this paper, the velocity and altitude control problem of hypersonic vehicles is studied. Aiming at the nonlinear parameter uncertainties, external disturbances and coupling of the hypersonic vehicle system, a control method combining backstepping control with linear active disturbance rejection control is proposed. The backstepping control solves the coupling of the system and transforms the longitudinal dynamic model of the hypersonic vehicle into the form of strict feedback, which is divided into the altitude subsystem and velocity subsystem. The linear extension state observer (LESO) can observe parameter uncertainty disturbance and external disturbance. At the same time, the stability of the system is proved by Lyapunov theory. Finally, the effectiveness of the designed controller is verified by numerical simulation and comparison with classical PID control.

Keywords: velocity and altitude control; hypersonic vehicle; backstepping control; classical PID control; linear extension state observer

1. Citation

Due to the advanced engine/body integration configuration of hypersonic vehicles, there is an obvious strong coupling relationship. At the same time, the large flight Mach number [1] makes the motion process of the hypersonic vehicle have strong nonlinear and fast time-varying characteristics, which brings many difficulties to controller design. Zhang et al. [2] put forward the active thermal protection of hypersonic aircraft in flight. Sun et al. [3] put forward the use of air propulsion and elevator-to-elevator coupling to design a hypersonic vehicle controller. Wang et al. [4] put forward a quasi-continuous high-order sliding mode (HOSM) controller based on full state feedback to track the step changes in speed and altitude. According to the characteristics of the longitudinal model, Li et al. [5] divided the aircraft model into two subsystems, including the altitude subsystem and the speed subsystem. Ding et al. [6] summarized the fault-tolerant control anti-saturation considering the external disturbance of aircraft and the specified performance control considering transient performance constraints.

In recent years, many scholars have conducted research on the design of hypersonic vehicle controllers. The literature [7] provides an overview of the current technical issues and challenges associated with the design of hypersonic vehicles. The cooperative guidance strategy of a multi-hypersonic vehicle system with flight constraints and cooperative constraints is proposed in the literature [8]. A variety of aircraft engine configurations using ABREAST are proposed in the literature [9]. Backstepping control, adaptive control [10], fuzzy control, robust control [11,12], synovial membrane control [13], etc., have been used in controller design and have achieved excellent results. The research by Rehman et al. [14] combined feedback linearization and optimal control to design a robust controller for general systems with parameter uncertainties. The research by Kamal et al. [15] designed a high-order super-warping algorithm, but the algorithm had too many controller parameters. The research by Wang et al. [16] designed a hypersonic vehicle control system using a synovial membrane disturbance observer and adaptive backstepping control. It achieved



Citation: Bao, C.; Zhu, G.; Zhao, T. Research on Backstepping Linear Active Disturbance Rejection Control of Hypersonic Vehicle. *Appl. Sci.* **2024**, *14*, 5367. <https://doi.org/10.3390/app14135367>

Academic Editor: Jérôme Morio

Received: 28 April 2024

Revised: 13 June 2024

Accepted: 17 June 2024

Published: 21 June 2024



Copyright: © 2024 by the authors. Licensee MDPI, Basel, Switzerland. This article is an open access article distributed under the terms and conditions of the Creative Commons Attribution (CC BY) license (<https://creativecommons.org/licenses/by/4.0/>).

good control effects. Backstepping control shows its unique advantages when designing the controller of a complex system. For example, hypersonic vehicles have parameter uncertainties such as variations and aerodynamic parameter uncertainties. Backstepping control can fully consider these influencing factors in the controller design, thus significantly improving the robustness of the system and ensuring the stable flight and precise control of the aircraft under various complexities [17]. In reference [18], a distributed actuator fault compensation scheme for a hypersonic vehicle is designed based on model transformation backstepping control, which improves the control accuracy in the case of actuator failure. However, these control methods still have shortcomings. In the face of random disturbances, the tracking error of the controller is relatively large. active disturbance rejection control (ADRC) can observe the disturbance, which greatly enhances the robustness of the system. Reference [19] proposes a 2-degree-of-freedom control based on an extended state observer for estimating and eliminating total disturbance. Reference [20] proposes the application of linear flatness control along with active disturbance rejection control (ADRC) for the local stabilization and trajectory tracking problems in the underactuated ball and rigid triangle system. An adaptive robust control device is proposed in reference [21]. A linear active disturbance rejection controller (LADRC) is designed for NMAMS single-axis trajectory tracking control in reference [22]. The literature [23] introduces the theory of ADRC. The research by Yan and Sun [24] designed a hypersonic vehicle controller based on ADRC. Considering the two situations of standard parameters and parameter perturbation in a large range, the control system can demonstrate good control performance. However, there are too many controller parameters in ADRC. Many intelligent optimization algorithms such as the foraging algorithm [25] and particle swarm algorithm [26,27] are used to optimize controller parameters. In the literature [28], a mass adaptive control method combining with robust sliding mode control (SMC) and linear active disturbance rejection control (LADRC) is designed for the quadrotor load unmanned aerial vehicle (UAV) with mass variation, but they are still difficult to adjust and have large parameter errors. An improved active disturbance rejection controller (ADRC) based on particle swarm optimization (PSO) is proposed to solve the problems of control accuracy, response speed and parameter tuning in the current dynamic communication antenna servo system [29]. A non-singular finite-time terminal sliding mode control is proposed in the literature [30]. The particle swarm optimization algorithm is used to obtain the design parameters of the proposed disturbance observer and controller. The literature [31] proposes an integrated filtered extended state filter into an active disturbance rejection control (ADRC) system and derives an improved ADRC. A general nonlinear ADRC algorithm is introduced in the literature [32].

The controller of a hypersonic vehicle needs a strong ability to restrain all kinds of disturbances in order to achieve higher control accuracy. Therefore, this paper uses a backstepping controller to make a more accurate nonlinear modeling of the system and uses an LADRC controller to observe and compensate for all kinds of disturbances of hypersonic vehicles. The main innovations of this paper are as follows:

1. Aiming at the strong coupling and nonlinearity of hypersonic vehicles, backstepping control is adopted to model the system close to the actual system model.
2. In view of the influence of unmodeled dynamic parameter disturbance and external disturbance on hypersonic vehicles in flight, the LESO is used to observe the disturbance.
3. In order to simulate the real flight of hypersonic vehicles, we consider the disturbance of the internal parameters of hypersonic vehicles and give the parameter fault tolerance range within 6%. We use Gaussian white noise to simulate the external disturbance in flight to reflect the randomness and uncertainty of the disturbance.

2. Basic Theory

Regarding the mathematical model of hypersonic vehicles, early research work includes a hypersonic vehicle model with a wing cone configuration given by the NASA Langley Research Center in 1990. This model has published most of the aerodynamic data of wind tunnel tests and has become the main model used by scholars around the world to design flight control systems [33]. It is shown as

$$\dot{V} = \frac{-D + T \cos \alpha}{m} - \frac{\sin \gamma}{r^2} \mu \tag{1}$$

$$\dot{\gamma} = \frac{T \sin \alpha + L}{mV} - \frac{(\mu - V^2 r) \cos \gamma}{Vr^2} \tag{2}$$

$$\dot{h} = V \sin \gamma \tag{3}$$

$$\dot{\alpha} = Q - \dot{\gamma} \tag{4}$$

$$\dot{Q} = \frac{M_{yy}}{I_{yy}} \tag{5}$$

where

$$L = 0.5\rho V^2 S C_L \tag{6}$$

$$D = 0.5\rho V^2 S C_D \tag{7}$$

$$T = 0.5\rho V^2 S C_T \tag{8}$$

$$M_{yy} = 0.5\rho V^2 S \bar{c} [C_M(\alpha) + C_M(\delta_c) + C_M(q)] \tag{9}$$

$$r = h + R_E \tag{10}$$

In Equations (1) through (10), V , γ , h , α and Q are the velocity, track angle, altitude, angle of attack and pitch rate, respectively. L , D , T and M_{yy} respectively represent lift, drag, thrust and pitching moment. m , μ , I_{yy} , r , R_E and S represent the mass of the hypersonic vehicle, gravitational constant, the moment of inertia, the radial distance from the center of the earth, the earth radius and the wing reference area, respectively. ρ represents the air density. \bar{c} is the aerodynamic mean chord length.

When cruising in the state, the expression of C_M is as follows:

$$C_L = 0.6203\alpha \tag{11}$$

$$C_D = 0.6450\alpha^2 + 0.0043378\alpha + 0.003772 \tag{12}$$

$$C_T = \begin{cases} 0.02576\beta_c, \beta_c < 1 \\ 0.0224 + 0.00336\beta_c, \beta_c \geq 1 \end{cases} \tag{13}$$

$$C_M(\alpha) = -0.035\alpha^2 + 0.036617\alpha + 5.3261 \times 10^{-6} \tag{14}$$

$$C_M(\delta_e) = c_e(\delta_e - \alpha) \tag{15}$$

$$C_M(Q) = 0.5 \frac{\bar{c} Q}{V} (-6.796\alpha^2 + 0.3015\alpha - 0.2289) \tag{16}$$

where c_e is the torque coefficient, and the control inputs are throttle opening command β_c and elevator deflection angle δ_e . For the multi-input and multi-output hypersonic vehicle system in which altitude and velocity are the most important state variables, if the control inputs and outputs are arranged as one-to-one correspondence, the ADRC has natural decoupling for the cross-coupling term between each channel. Based on the literature, the longitudinal dynamic model of the hypersonic vehicle is deformed and deformed into a form in which the velocity subsystem and the altitude subsystem are coupled with each other with a clear order. The parameters of the hypersonic vehicle used in this article are shown in Table 1.

Table 1. Parameters of the hypersonic vehicle.

Parameter	Description	Value	Unit
m	Quality	137,800	kg
I_{yy}	Y-axis moment of inertia	9,500,000	kg/m ³
S	Reference area	335.2	m ²
\bar{c}	Average aerodynamic chord length	24.384	m
ρ	Atmospheric density	0.0125368	kg/m ³
R_E	Earth radius	6,371,393	m

2.1. Velocity Subsystem

For the throttle opening $\beta_c = 0.1762$ at the equilibrium point, condition $\beta_c < 1$ is satisfied, so Equations (8) and (13) are brought into the speed control loop in the speed Expression (1), as shown in Equation (17):

$$\begin{cases} \dot{V} = f_V + g_V \beta_c \\ y_V = V \end{cases} \tag{17}$$

where $g_V = \frac{0.01288 \cos \alpha \rho V^2 S}{m}$ and $f_V = -\frac{Dr^2 - 2m\mu \sin \gamma}{2mr^2}$. In addition, if $\beta \geq 1$ is considered, $g_V = \frac{0.0018 \cos \alpha \rho V^2 S}{m}$ and $f_V = \frac{0.00224 \rho V^2 S \cos \alpha r^2 - Dr^2 - 2m\mu \sin \gamma}{2mr^2}$. It can be seen from Equation (17) that the speed subsystem takes the throttle opening β_c as the control input and the flight speed V as the output, which is a typical first-order system.

2.2. Altitude Subsystem

The altitude subsystem consists of a pitch angle loop, track angle loop and altitude loop.

2.2.1. Track Angle Loop

By modifying Equation (2), the track angle loop can be expressed as a first-order system, as shown in Equation (18).

$$\begin{cases} \dot{\gamma} = f_\gamma + g_\gamma \theta \\ y_\gamma = \gamma \end{cases} \tag{18}$$

where $f_\gamma = \frac{T \sin \alpha - 0.31015 \rho V^2 S \gamma}{mV} - \frac{(\mu - V^2 r \cos \gamma)}{V^2 r^2}$ and $g_\gamma = \frac{0.31015 \rho V^2 S}{mV}$.

2.2.2. Altitude Loop

The expression of the height loop is Equation (3). Taking height as output, the expression becomes the following:

$$\begin{cases} \dot{h} = V \sin \gamma \\ y_h = h \end{cases} \tag{19}$$

Here, because γ is small, there is $\gamma \approx \sin \gamma$, and the altitude loop can be regarded as a first-order system with track angle as input.

2.2.3. Pitch Angle Loop

According to Equations (2) and (4), the pitch angle loop can be expressed as a second-order system shown in the following Equation (20).

$$\begin{cases} \dot{\theta} = \dot{\alpha} + \dot{\gamma} = Q \\ \dot{Q} = f_Q + g_Q \delta_e \\ y_Q = \theta \end{cases} \quad (20)$$

$$f_Q = \frac{0.5}{I_{yy}} \left(\rho V^2 S \bar{c} \left(-\frac{3.398 \bar{c} Q}{V} - 0.035 \right) \alpha^2 + \left(\frac{0.15075 \bar{c} Q}{V} - 0.963383 - c_e \right) \alpha - \frac{0.11445 \bar{c} Q}{V} + 5.3261 \times 10^{-6} \right),$$

$$g_Q = \frac{0.5}{I_{yy}} \rho V^2 S \bar{c} c_e.$$

3. Proposed Methods

3.1. Theoretical Basis of Backstepping Control

Backstepping control is a kind of nonlinear control used to solve the control problem of a nonlinear system. Based on the recursive idea, the nonlinear system is transformed into a series of linear subsystems by designing virtual controllers and virtual variables step by step, and linear controllers are designed to control these subsystems, thus realizing the control of the whole nonlinear system. Firstly, based on the principle of feedback linearization, the longitudinal dynamic model of a hypersonic vehicle is transformed into strict feedback form and divided into the altitude subsystem and velocity subsystem. In view of the disturbance existing in the altitude and velocity subsystems, the LESO is used to estimate the disturbance and improve the anti-interference ability of the system.

The general steps of backstepping controller design are as follows [34]:

Define the state and control inputs of the system. Determine the state variables and control input variables of the system.

- (1) Designing virtual controllers and virtual variables: According to the characteristics and control requirements of the system, a virtual controller and corresponding virtual variables are designed. By introducing these virtual variables, the original nonlinear system is transformed into a new nonlinear system.
- (2) Designing a linear controller: Based on the new nonlinear system, a linear controller is designed to make the output requirements of the subsystem. Linear controls such as LQR (Linear Quadratic Regulation) or PID (Proportional Integral Differential) controllers can be used.
- (3) Iterative design: According to the complexity and control requirements of the system, it may be necessary to design a virtual controller and linear controller iteratively for many times until the control requirements of the whole nonlinear system are met.
- (4) Implementation controller: The designed controller is implemented in the actual system.

In the backstepping controller design, the speed subsystem and the height subsystem are designed, respectively. There is only one step in the design of the speed subsystem controller. The controller design of the altitude subsystem is divided into four steps according to the order of altitude, track angle, pitch angle, pitch angle, rate and elevator deflection angle. The structural diagram of the system is shown in Figure 1.

In order to further improve the control accuracy of the system, a backstepping control law is designed for height and speed subsystems to replace LSEF in LADRC to realize on-line disturbance compensation. Figure 2 is a backstepping LADRC control structure diagram taking a second-order system as an example.

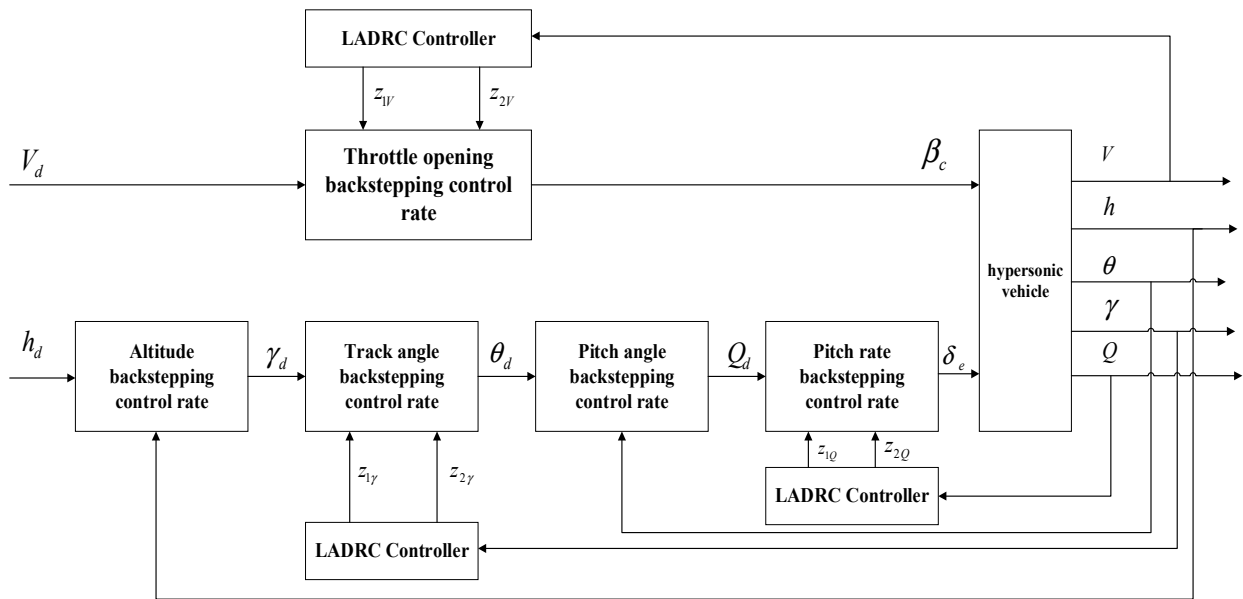


Figure 1. Hypersonic aircraft backstepping LADRC control system structure diagram.

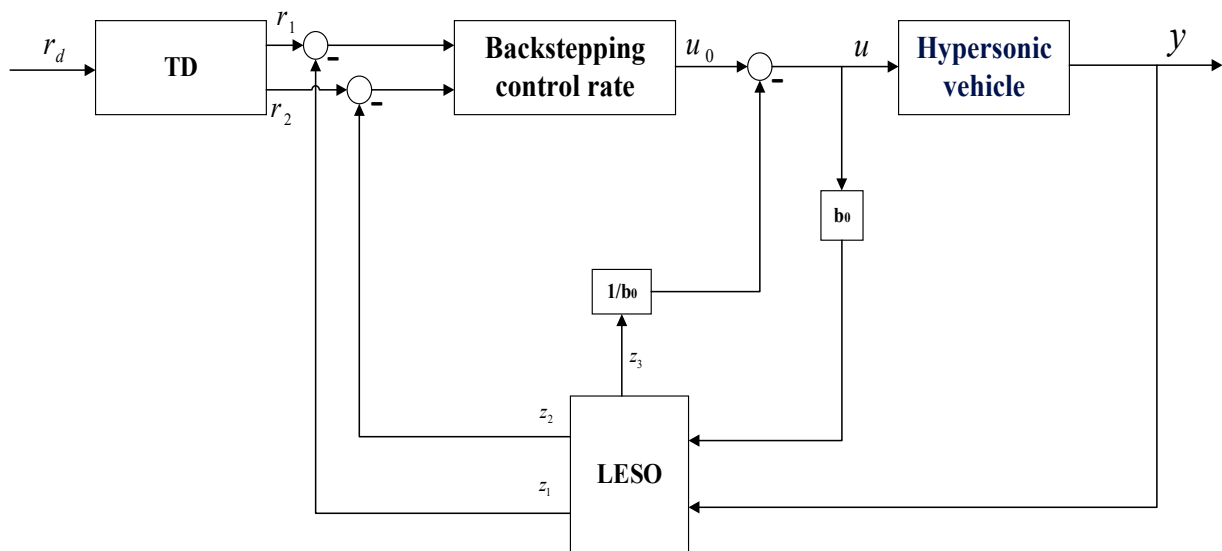


Figure 2. Backstepping LADRC control structure diagram.

3.2. Design of Backstepping Linear Active Disturbance Rejection Controller

3.2.1. Controller Design of Velocity Subsystem

For Equation (17), take the velocity error: $e_V = V - V_d$, where V_d is the reference velocity trajectory, and V is the actual velocity trajectory, and then derive the velocity tracking error as follows:

$$\dot{e}_V = \dot{V} - \dot{V}_d \tag{21}$$

Bringing Equation (17) into Equation (21),

$$\dot{e}_V = f_V + g_V \beta_c - \dot{V}_d \tag{22}$$

The controllable rate of the combination of Formulas (21) and (22) is the following:

$$\beta_c = \frac{1}{g_V} (\dot{V}_d - f_V - c_1 e_V) \tag{23}$$

where c_1 is an adjustable normal number.

The velocity subsystem represented by the definition $x_{1V} = V$ and $x_{2V} = \dot{f}_V$ in Equation (17) can be expressed in the form of the following state space expression:

$$\begin{cases} \dot{x}_{1V} = x_{2V} + g_V \beta_c \\ \dot{x}_{2V} = \dot{f}_V \\ y_V = x_{1V} \end{cases} \quad (24)$$

The state variables of the system represented by Equation (24) are observed using the LESO. The observation equation of the LESO is shown by the following Equation (25):

$$\begin{cases} \varepsilon_V = z_1 - y_V \\ \dot{z}_{1V} = z_{2V} - \beta_{01}^V \varepsilon_V + g_V \beta_c \\ \dot{z}_{2V} = -\beta_{02}^V \varepsilon_V \end{cases} \quad (25)$$

The tracking of the state variables of the original system (24) can be realized when the system reaches stability through the observation of the LESO. According to Equations (23) and (25), the controllable rate is as follows:

$$\beta_c = \frac{1}{g_V} (\dot{V}_d - z_{2V} - c_1 \varepsilon_V) \quad (26)$$

3.2.2. Design of Height Subsystem Controller

(1) Design of Height Loop Controller

For Equation (19), take the height error: $e_h = h - h_d$, where h_d is the reference height trajectory, and h is the actual height trajectory, and then derive the height tracking error:

$$\dot{e}_h = \dot{h} - \dot{h}_d \quad (27)$$

Bringing Equation (19) into Equation (27),

$$\dot{e}_h = V\gamma - \dot{h}_d \quad (28)$$

The controllable rate of the combination of Formulas (27) and (28) is as follows:

$$\gamma_d = \frac{\dot{h}_d - c_2 e_h}{V} \quad (29)$$

where c_2 is an adjustable normal number.

(2) Design of Track Angle Loop Controller

For Equation (18), take the track angle error: $e_\gamma = \gamma - \gamma_d$, where γ_d is the reference track angle trajectory, and γ is the actual track angle trajectory, and then derive the track angle tracking error:

$$\dot{e}_\gamma = \dot{\gamma} - \dot{\gamma}_d \quad (30)$$

Bringing Equation (18) into Equation (30),

$$\dot{e}_\gamma = g_\gamma \theta + f_\gamma - \dot{\gamma}_d \quad (31)$$

The controllable rate of the combination of Formulas (19) and (20) is as follows:

$$\theta_d = \frac{1}{g_\gamma} (\dot{\gamma}_d - f_\gamma - c_3 e_\gamma) \quad (32)$$

where c_3 is an adjustable normal number.

The track angle subsystem represented by the definition $x_{1\gamma} = \gamma$ and $x_{2\gamma} = \dot{\gamma}$ in Equation (18) can be expressed in the form of the following state space expression:

$$\begin{cases} \dot{x}_{1\gamma} = x_{2\gamma} + g_\gamma \theta \\ \dot{x}_{2\gamma} = \dot{f}_\gamma \\ y_\gamma = x_{1\gamma} \end{cases} \quad (33)$$

The state variables of the system represented by Equation (33) are observed using the LESO. The observation equation of the LESO is shown by the following Equation (34):

$$\begin{cases} \varepsilon_\gamma = z_{1\gamma} - y_\gamma \\ \dot{z}_{1\gamma} = z_{2\gamma} - \beta_{01}^\gamma \varepsilon_\gamma + g_\gamma \theta \\ \dot{z}_{2\gamma} = -\beta_{02}^\gamma \varepsilon_\gamma \end{cases} \quad (34)$$

The tracking of the state variables of the original system (33) can be realized when the system reaches stability through the observation of the LESO. According to Equations (32) and (34), the controllable rate is as follows:

$$\theta_d = \frac{1}{g_\gamma} (\dot{\gamma}_d - z_{2\gamma} - c_3 \varepsilon_\gamma) \quad (35)$$

(3) Design of Pitch Angle Loop Controller

For Equation (20), take the pitch angle error: $e_\theta = \theta - \theta_d$, where θ_d is the reference pitch angle trajectory, and θ is the actual pitch angle trajectory, and then derive the pitch angle tracking error:

$$\dot{e}_\theta = \dot{\theta} - \dot{\theta}_d \quad (36)$$

Bringing Equation (20) into Equation (36),

$$\dot{e}_\theta = Q - \dot{\theta}_d \quad (37)$$

The controllable rate of the combination of Formulas (36) and (37) is as follows:

$$Q_d = \dot{\theta}_d - c_4 e_\theta \quad (38)$$

where c_4 is an adjustable normal number.

(4) Design of Pitch Angle Rate Loop Controller

For Equation (20), take the pitch angle rate error: $e_Q = Q - Q_d$, where Q_d is the reference pitch angle rate trajectory, and Q is the actual pitch angle rate trajectory, and then derive the pitch angle rate tracking error:

$$\dot{e}_Q = \dot{Q} - \dot{Q}_d \quad (39)$$

Bringing Equation (20) into Equation (39),

$$\dot{e}_Q = g_Q \delta_e + f_Q - \dot{Q}_d \quad (40)$$

The controllable rate of the combination of Formula (39) and Formula (40) is as follows:

$$\delta_e = \frac{\dot{Q}_d - f_Q - c_5 e_Q}{g_Q} \quad (41)$$

where c_5 is an adjustable normal number.

The pitch angle rate subsystem represented by the definition $x_{1Q} = Q$ and $x_{2Q} = \dot{Q}$ in Equation (20) can be expressed in the form of the following state space expression:

$$\begin{cases} \dot{x}_{1Q} = x_{2Q} + g_Q \delta_e \\ \dot{x}_{2Q} = f_Q \\ y_Q = x_{1Q} \end{cases} \quad (42)$$

The state variables of the system represented by Equation (42) are observed using the LESO. The observation equation of the LESO is shown by the following Equation (43):

$$\begin{cases} \varepsilon_Q = z_{1Q} - y_Q \\ \dot{z}_{1Q} = z_{2Q} - \beta_{01}^Q \varepsilon_Q + g_Q \delta_e \\ \dot{z}_{2Q} = -\beta_{02}^Q \varepsilon_Q \end{cases} \quad (43)$$

The tracking of the state variables of the original system (42) can be realized when the system reaches stability through the observation of the LESO. According to Equations (41) and (43), the controllable rate is as follows:

$$\delta_e = \frac{\dot{Q}_d - z_{2Q} - c_5 e_Q}{g_Q} \quad (44)$$

4. Proof of Stability

4.1. Proof of Stability of Velocity Subsystem

The Lyapunov function is defined as follows for the velocity subsystem:

$$V_V = \frac{1}{2} e_V^2 \quad (45)$$

By deriving the above formula, we can obtain the following:

$$\dot{V}_V = \dot{e}_V e_V \quad (46)$$

Bringing Equations (22) and (26) into Equation (46),

$$\begin{aligned} \dot{V}_V &= e_V (f_V + g_V \beta_c - \dot{V}_d) \\ &= e_V [f_V + g_V \frac{1}{g_V} (\dot{V}_d - z_{2V} - c_1 e_V) - \dot{V}_d] \\ &= e_V (f_V - z_{2V} - c_1 e_V) \\ &= -c_1 e_V^2 \leq 0 \end{aligned} \quad (47)$$

According to Lyapunov stability, the velocity subsystem is uniformly stable. Simultaneously, it can also be proved that the velocity error e_V and its differential \dot{e}_V are bounded.

According to Barbalat theorem, if the e_V and \dot{e}_V are bounded and e_V is square integrable, the following formula holds:

$$\lim_{t \rightarrow \infty} e_V(t) = 0 \quad (48)$$

According to Equation (47), Equation (45) is a bounded and decreasing function, which can be derived:

$$\int_0^\infty e_V^2(t) dt = [V_V(0) - V_V(\infty)] / l < \infty \quad (49)$$

According to Formula (49), e_V is square integrable. At the same time, e_V and \dot{e}_V are bounded. Therefore, the speed tracking error converges to 0, and the speed subsystem is asymptotically stable.

4.2. Proof of Stability of Altitude Subsystem

The Lyapunov function is defined as follows for the altitude subsystem:

$$V_h = \frac{1}{2}e_h^2 + \frac{1}{2}e_\gamma^2 + \frac{1}{2}e_\theta^2 + \frac{1}{2}e_Q^2 \tag{50}$$

By deriving the above formula, we can obtain the following:

$$\dot{V}_h = e_h\dot{e}_h + e_\gamma\dot{e}_\gamma + e_\theta\dot{e}_\theta + e_Q\dot{e}_Q \tag{51}$$

Bringing Equations (28), (29), (31), (35), (37), (38), (40) and (44) into Equation (51),

$$\begin{aligned} \dot{V}_h &= e_h(V\gamma - \dot{h}_d) + e_\gamma(g_\gamma\theta + f_\gamma - \dot{\gamma}_d) + e_\theta(Q - \dot{\theta}_d) + e_Q(g_Q\delta_e + f_Q - \dot{Q}_d) \\ &= -c_2e_h^2 - c_3e_\gamma^2 - c_4e_\theta^2 - c_5e_Q^2 \leq 0 \end{aligned} \tag{52}$$

According to Lyapunov stability, the altitude subsystem is uniformly stable. Simultaneously, it can also be proved that everything in the altitude subsystem is bounded.

According to Function (52), Function (50) is a bounded and decreasing function, which can be derived as follows:

$$\int_0^\infty [e_h^2(t) + e_\gamma^2(t) + e_\theta^2(t) + e_Q^2(t)]dt = [V_h(0) - V_h(\infty)]/l < \infty \tag{53}$$

According to Formula (53), e_h , e_γ , e_θ and e_Q are square integrable. Therefore, the altitude tracking error converges to 0, and the altitude subsystem is asymptotically stable.

5. Simulation and Analysis

In order to avoid a given mutation in height and speed, the prefilters are used to generate the velocity and altitude commands of the hypersonic vehicle in this paper:

$$V_d = (V_c - V_0) \times \frac{\lambda^2}{s^2 + 2\mu\lambda s + \lambda^2} + V_0 \tag{54}$$

$$h_d = (h_c - h_0) \times \frac{\lambda^2}{s^2 + 2\mu\lambda s + \lambda^2} + h_0 \tag{55}$$

where μ and λ are the filter parameters; V_0 and h_0 are the initial velocity and altitude of the aircraft; V_c and h_c are the given step reference. The function of the prefilter is to modulate the step V_c , h_c into V_d , h_d .

The initial simulation values of the hypersonic vehicle are shown in Table 2 below.

Table 2. Initial simulation values of hypersonic vehicle.

Parameter	Description	Value	Unit
V_0	Initial value of velocity	4590	m/s
γ_0	Initial value of track angle	0	deg
h_0	Initial value of altitude	33,528	m
α_0	Initial value of angle of attack	2.745	deg
Q_0	Initial value of pitch angular rate	0	deg/s

Example 1. In order to verify the effectiveness of the algorithm proposed in this paper, the speed and altitude reference tracking is carried out without interference. The control strategy requires a speed of 50 m/s and a height of 200 m. The controller parameters are shown in the following Table 3. In order to verify the superior performance of the controller designed in this paper, the classical PID controller is adopted to track the speed and altitude of the aircraft, which is the same as above. The

PID controller parameter settings are shown in Table 4. Finally, the tracking performance of the two controllers in altitude and speed channels is compared.

Table 3. Controller parameters.

Parameter	Value	Parameter	Value
β_{01}^V	120	c_1	1
β_{02}^V	4800	c_2	1
β_{01}^Y	50	c_3	2
β_{02}^Y	7500	c_4	2
β_{01}^Q	90	c_5	2
β_{02}^Q	2700		

Table 4. PID Controller parameters.

Parameter	Value	Parameter	Value
k_p^h	1	k_p^V	1
k_i^h	0.1	k_i^V	0.1
k_d^h	0.05	k_d^V	0.05

It can be seen that the speed and altitude can track the given speed and altitude stably without interference. It can be seen from the height tracking curve in Figure 3 that the two controllers have reached the preset height at last, but BSLADRC obviously has a better tracking effect than PID. Before 90 s, the PID tracking effect is not as good as the BSLADRC tracking effect and has obvious error, and BSLADRC has smaller overshoot than PID, almost no overshoot and can quickly reach a stable state. From the speed tracking curve in Figure 4, we can see the two controllers have reached the preset velocity at last, but BSLADRC obviously has a better tracking effect than PID. Before 90 s, the PID tracking effect is not as good as the BSLADRC tracking effect and has obvious error, and BSLADRC has smaller overshoot than PID, almost no overshoot and can quickly reach a stable state. Figure 5 shows that the tracking curve of the track angle converges to the steady state value in about 1.2 s after the given speed change and altitude change instructions, which shows that the controller can control and track the track angle quickly and reach the steady state quickly. Figure 6 shows the tracking curve of the angle of attack. The curve shows that it converges to the steady state value in about 2.7 s; that is, the aircraft can stabilize its attitude in about 2.7 s so that it can fly stably; that is, it can quickly reach the steady state of flight. Figure 7 shows that both controllers can finally reach a steady state, but the error of BSLADRC can converge to 0 faster. The fluctuation before 40 s of BSLADRC indicates that the aircraft will be affected by some disturbances inside the aircraft during the ascent stage, so it will lead to fluctuations. After reaching the steady state value, the stable flight of the aircraft can be realized; that is, the designed controller can make the aircraft rise to the preset altitude. However, the time for PID to reach stability is too long, and the error is also very large, so BSLADRC has better performance and stability than PID control. Figure 8 shows the tracking curve of speed error. The curve shows that BSLADRC converges faster than PID, and it can reach the stable value for 1 s. After reaching the stable value, it can realize the stable flight of the aircraft; that is, the designed controller can accelerate the aircraft to the preset speed and then rise the aircraft to the preset altitude. But PID takes a longer time to reach steady state and has a large error, so BSLADRC has better performance and stability than PID control.

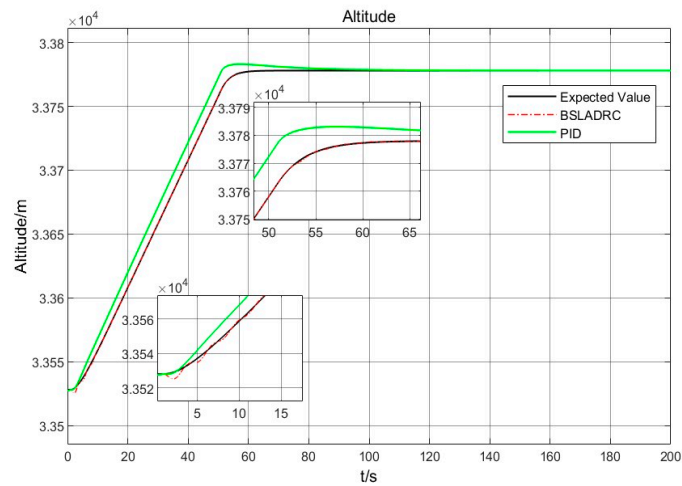


Figure 3. Altitude tracking curve.

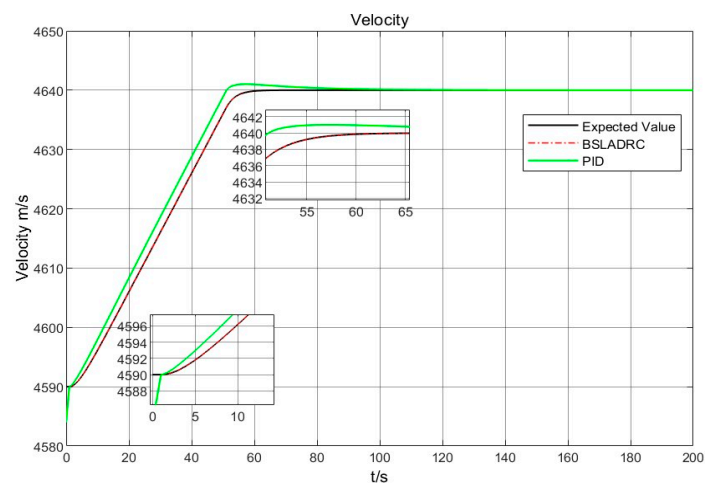


Figure 4. Velocity tracking curve.

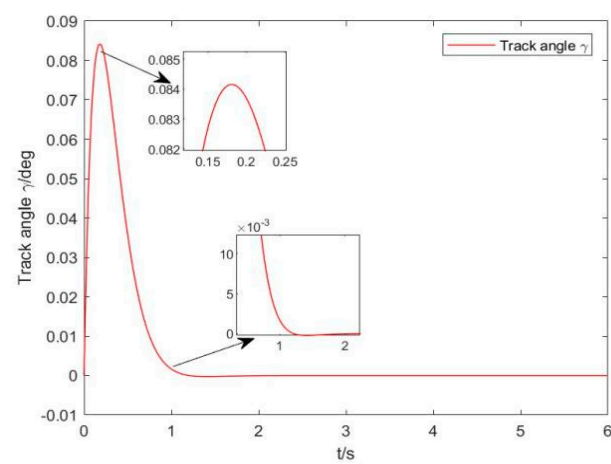


Figure 5. Track angle tracking curve.

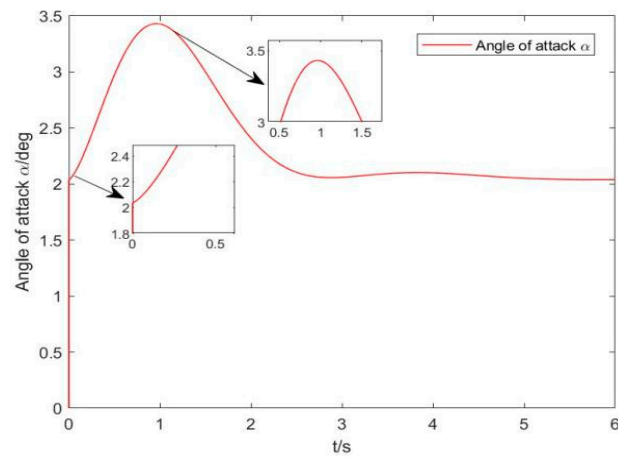


Figure 6. Angle of attack tracking curve.

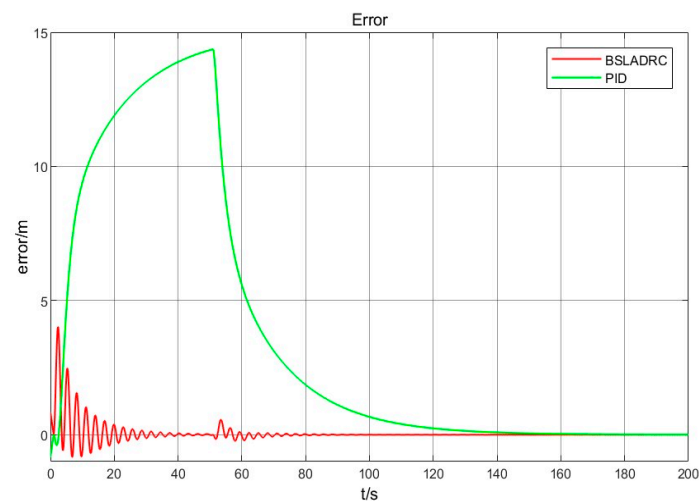


Figure 7. Altitude tracking error curve.

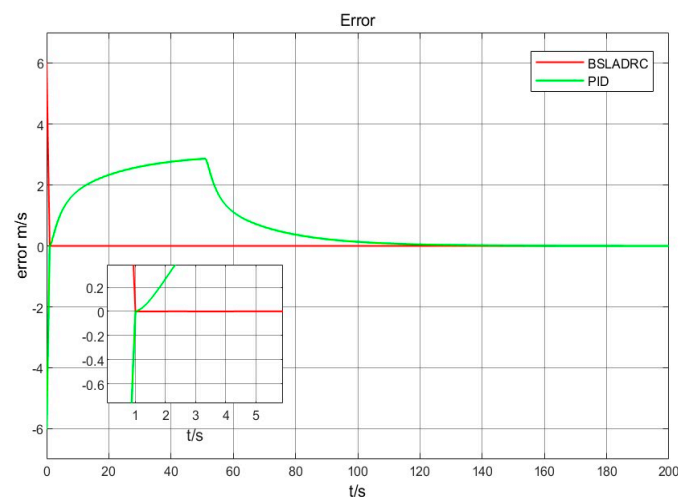


Figure 8. Velocity tracking error curve.

Example 2. Considering that the hypersonic vehicle may be subjected to various unknown random disturbances in flight, they will affect the stability of the system. In order to verify the anti-jamming ability of the proposed algorithm against random disturbances, white Gaussian noise with a mean value of 0 and variance of 2.5 is used as the noise jamming of the hypersonic vehicle system in this

simulation test. The control strategy is the same as the requirements of Example 1. Figure 9 is a Gaussian white noise curve. The controller parameters are the same as those set in Example 1. The PID controller parameter settings are the same as in Example 1.

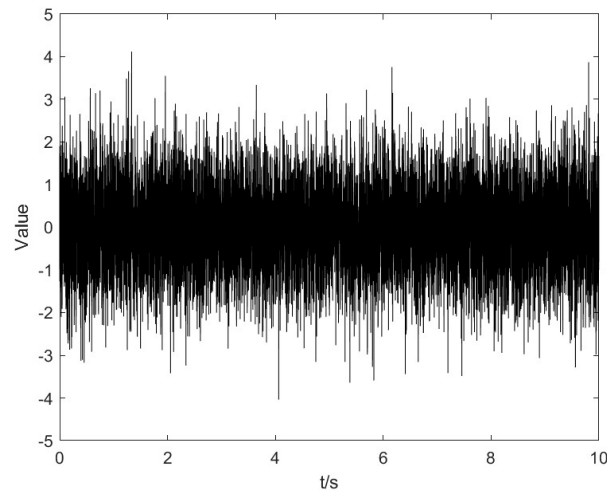


Figure 9. Gaussian white noise curve.

It can be seen that both speed and altitude can track the given speed and altitude instructions stably under the condition of interference. From the altitude tracking curves in Figure 10, it can be seen that the two controllers have reached the preset height at last, but BSLADRC obviously has a better tracking effect than PID. Before 80 s, the PID tracking effect is not as good as the BSLADRC tracking effect and has obvious error, and BSLADRC has smaller overshoot than PID, almost no overshoot and can quickly reach a stable state. From the velocity tracking curves in Figure 11, it can be seen that we can see the two controllers have reached the preset velocity at last, but BSLADRC obviously has a better tracking effect than PID. Before 90 s, the PID tracking effect is not as good as the BSLADRC tracking effect and has obvious error, and BSLADRC has smaller overshoot than PID, almost no overshoot and can quickly reach a stable state. Figure 12 shows that both controllers can finally reach a steady state, but the error of BSLADRC can converge to 0 faster. The fluctuation before 40 s of BSLADRC indicates that the aircraft will be affected by some disturbances inside the aircraft during the ascent stage, so it will lead to fluctuations. After reaching the steady state value, the stable flight of the aircraft can be realized; that is, the designed controller can make the aircraft rise to the preset altitude. However, the time for PID to reach stability is too long, and the error is also very large, and the error fluctuates between -5 and 5 all the time, so BSLADRC has better performance and stability than PID control. Figure 13 shows the tracking curve of speed error. The curve shows that BSLADRC converges faster than PID, and it can reach the stable value for 1 s. After reaching the stable value, it can realize the stable flight of the aircraft; that is, the designed controller can accelerate the aircraft to the preset speed and then rise the aircraft to the preset altitude. But PID takes a longer time to reach steady state and has a large error, so BSLADRC has better performance and stability than PID control. The simulation results show that the designed controller has a strong ability to suppress the disturbance under the influence of Gaussian white noise disturbance, which enhances the anti-interference ability of the system. Compared with the classical PID control, the control accuracy of the system is improved, and the robustness of the system is enhanced.

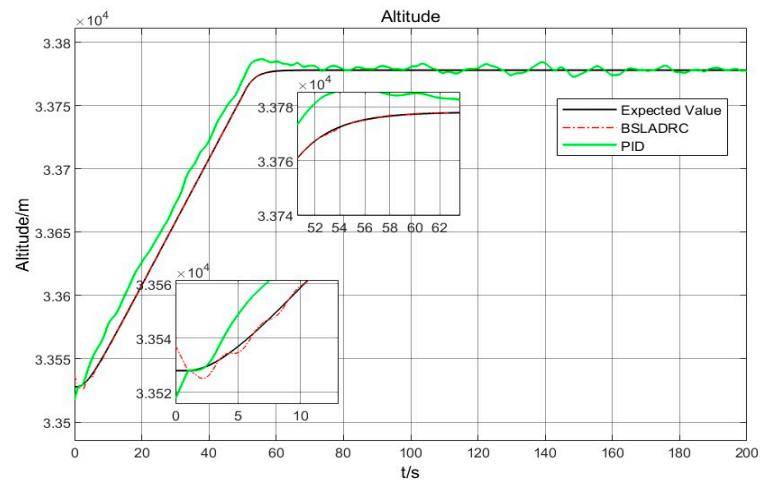


Figure 10. Altitude tracking curve with interference.

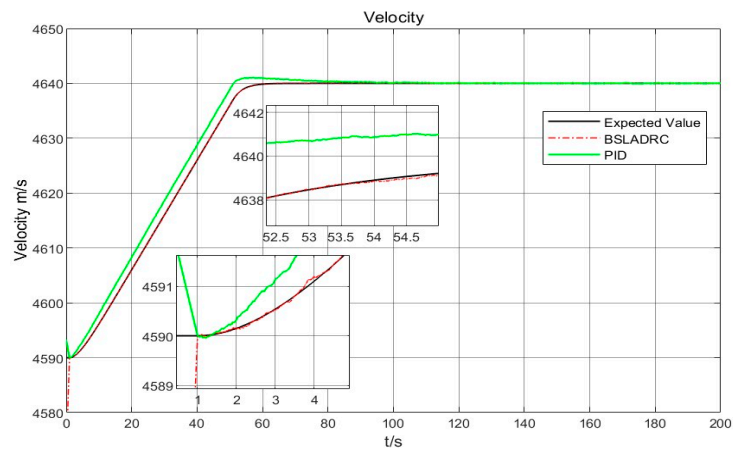


Figure 11. Velocity tracking curve with interference.

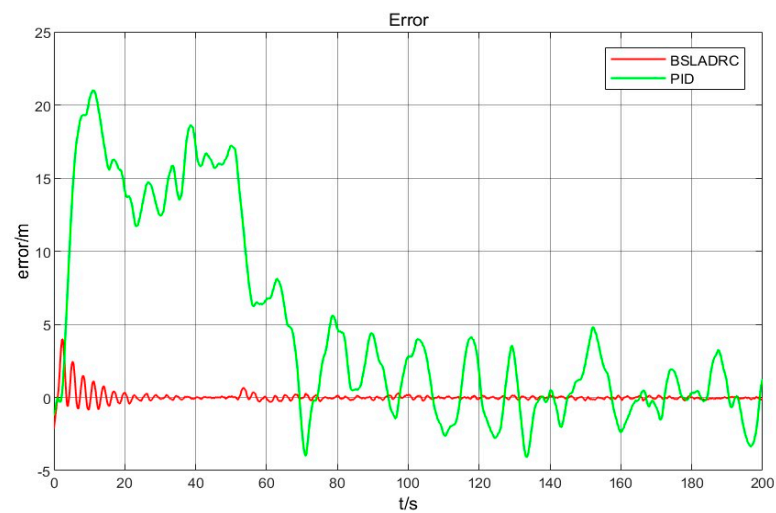


Figure 12. Altitude tracking error curve with interference.

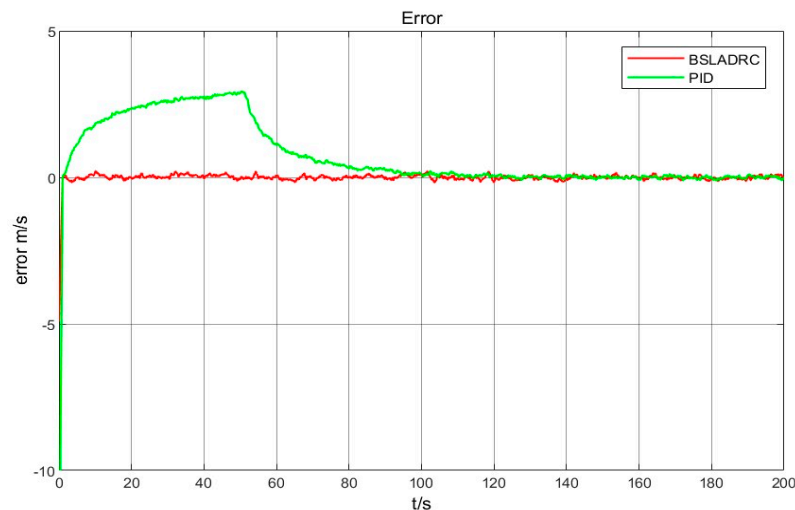


Figure 13. Velocity tracking error curve with interference.

6. Conclusions

Based on backstepping control and active disturbance rejection theory, the velocity and altitude tracking problem of hypersonic vehicles under the influence of internal parameter uncertainties and external disturbances is studied. The main results are as follows:

- (1) The LADRC controller is designed based on the ADRC theory. The LESO can effectively compensate the total disturbance suffered by the hypersonic vehicle.
- (2) By designing a backstepping control law instead of LSEF in LADRC, it is realized on-line compensation for disturbance.
- (3) The stability is demonstrated using Lyapunov stability theory. Compared with the classical PID control, the control scheme proposed in this paper can overcome the adverse effects brought by external uncertainties and track the control instructions stably and accurately without overshoot; whether from the point of view of control accuracy or error, the control scheme proposed in this paper can ensure the accurate tracking of the given and can ensure almost no overshoot, can ensure its control accuracy and improve the robustness of the control system compared with the classical PID control.

At present, this paper is limited to theoretical analysis. Although it is widely used and has difficult to adjust parameters in classical PID control, the control accuracy will be greatly reduced in the face of nonlinear complex system similar to a hypersonic vehicle, and it is not suitable for the precise control of this nonlinear complex system. For the control scheme proposed in this paper, although it solves the nonlinear modeling of the model and improves the anti-interference ability of the system, this modeling depends on the accuracy of the model. Because the control rate is established based on the mathematical model of the system itself, if the mathematical model of the system is inaccurate, it is similar to the approximate or simplified mathematical model. This scenario will not be applicable to this type of model. In addition, the actual flight of aircraft is much more complicated than the simulation, so this paper only carries out an approximate simulation. Subsequent work will be carried out to study more complex simulation to further enhance the control performance of the proposed seven-point control system.

Author Contributions: Conceptualization, C.B.; Software, T.Z.; Validation, C.B.; Resources, T.Z.; Data curation, C.B. and G.Z.; Writing—original draft, C.B.; Writing—review & editing, T.Z.; Visualization, G.Z.; Supervision, G.Z.; Project administration, T.Z. All authors have read and agreed to the published version of the manuscript.

Funding: This research received no external funding.

Institutional Review Board Statement: Not applicable.

Informed Consent Statement: Not applicable.

Data Availability Statement: The data presented in this study are available on request from the corresponding author. The data are not publicly available due to privacy.

Conflicts of Interest: The authors declare that they have no competing interests.

References

1. McFarland, J. The Development of Hypersonic Weapons in the US, China and Russia: An Incipient Arms Race. *RUSI J.* **2023**, *168*, 10–18. [\[CrossRef\]](#)
2. Zhang, S.; Li, X.; Zuo, J.; Qin, J.; Cheng, K.; Feng, Y.; Bao, W. Research progress on active thermal protection for hypersonic vehicles. *Prog. Aerosp. Sci.* **2020**, *119*, 100646. [\[CrossRef\]](#)
3. Sun, H.; Yang, Z.; Zeng, J. New tracking-control strategy for airbreathing hypersonic vehicles. *J. Guid. Control. Dyn.* **2013**, *36*, 846–859. [\[CrossRef\]](#)
4. Wang, J.; Zong, Q.; Tian, B.; Liu, H. Flight control for a flexible air-breathing hypersonic vehicle based on quasi-continuous high-order sliding mode. *J. Syst. Eng. Electron.* **2013**, *24*, 288–295. [\[CrossRef\]](#)
5. Li, S.; Sun, H.; Sun, C. Composite controller design for an air-breathing hypersonic vehicle. *Proc. Inst. Mech. Eng. Part I J. Syst. Control. Eng.* **2012**, *226*, 651–664. [\[CrossRef\]](#)
6. Yibo, D.; Xiaokui, Y.U.; Guangshan, C.H.; Jiashun, S.I. Review of control and guidance technology on hypersonic vehicle. *Chin. J. Aeronaut.* **2022**, *35*, 1–18.
7. Sziroczak, D.; Smith, H. A review of design issues specific to hypersonic flight vehicles. *Prog. Aerosp. Sci.* **2016**, *84*, 1–28. [\[CrossRef\]](#)
8. Yu, J.; Dong, X.; Li, Q.; Ren, Z.; Lv, J. Cooperative guidance strategy for multiple hypersonic gliding vehicles system. *Chin. J. Aeronaut.* **2020**, *33*, 990–1005. [\[CrossRef\]](#)
9. Clark, A.; Wu, C.; Mirmirani, M.; Choi, S.B.; Kuipers, M. Development of an airframe-propulsion integrated hypersonic vehicle model. In Proceedings of the 44th AIAA Aerospace Sciences Meeting and Exhibit, Reno, Nevada, 9 January 2006; p. 218.
10. Ding, Y.; Wang, X.; Bai, Y.; Cui, N. Adaptive higher order super-twisting control algorithm for a flexible air-breathing hypersonic vehicle. *Acta Astronaut.* **2018**, *152*, 275–288. [\[CrossRef\]](#)
11. Zhao, Z.-T.; Huang, W.; Yan, L.; Yang, Y.-G. An overview of research on wide-speed range waverider configuration. *Prog. Aerosp. Sci.* **2020**, *113*, 100606. [\[CrossRef\]](#)
12. Boyi, C.H.; Yanbin, L.I.; Haidong, S.H.; Hao, L.E.; Yuping, L.U. Performance limitations in trajectory tracking control for air-breathing hypersonic vehicles. *Chin. J. Aeronaut.* **2019**, *32*, 167–175.
13. Ding, Y.; Wang, X.; Bai, Y.; Cui, N. An improved continuous sliding mode controller for flexible air-breathing hypersonic vehicle. *Int. J. Robust Nonlinear Control* **2020**, *30*, 5751–5772. [\[CrossRef\]](#)
14. Rehman, O.U.; Fidan, B.; Petersen, I.R. Robust minimax optimal control of nonlinear uncertain systems using feedback linearization with application to hypersonic flight vehicles. In Proceedings of the 48th IEEE Conference on Decision and Control (CDC) Held Jointly with 2009 28th Chinese Control Conference, Shanghai, China, 15–18 December 2009; pp. 720–726.
15. Kamal, S.; Chalanga, A.; Moreno, J.A.; Fridman, L.; Bandyopadhyay, B. Higher order super-twisting algorithm. In Proceedings of the 2014 13th International Workshop on Variable Structure Systems (VSS), Nantes, France, 29 June–2 July 2014; pp. 1–5.
16. An, H.; Wang, C.; Fidan, B. Sliding mode disturbance observer-enhanced adaptive control for the air-breathing hypersonic flight vehicle. *Acta Astronaut.* **2017**, *139*, 111–121. [\[CrossRef\]](#)
17. Vaidyanathan, S.; Azar, A.T. (Eds.) *Backstepping Control of Nonlinear Dynamical Systems*; Academic Press: New York, NY, USA, 2020.
18. Zhao, D.; Jiang, B.; Yang, H. Backstepping-based decentralized fault-tolerant control of hypersonic vehicles in PDE-ODE form. *IEEE Trans. Autom. Control.* **2021**, *67*, 1210–1225. [\[CrossRef\]](#)
19. Xue, W.; Huang, Y. Performance analysis of 2-DOF tracking control for a class of nonlinear uncertain systems with discontinuous disturbances. *Int. J. Robust Nonlinear Control* **2018**, *28*, 1456–1473. [\[CrossRef\]](#)
20. Aguilar-Ibanez, C.; Sira-Ramirez, H.; Suarez-Castanon, M.S. A linear active disturbance rejection control for a ball and rigid triangle system. *Math. Probl. Eng.* **2016**, *2016*, 1358930. [\[CrossRef\]](#)
21. Guo, Y.; Cheng, W.; Gong, D.; Zhang, Y.; Zhang, Z.; Xue, G. Adaptively robust rotary speed control of an anchor-hole driller under varied surrounding rock environments. *Control. Eng. Pr.* **2019**, *86*, 24–36. [\[CrossRef\]](#)
22. Wang, Y.W.; Zhang, W.A.; Dong, H.; Yu, L. A LADRC based fuzzy PID approach to contour error control of networked motion control system with time-varying delays. *Asian J. Control* **2020**, *22*, 1973–1985. [\[CrossRef\]](#)
23. Huang, Y.; Xue, W.; Yang, X. Active disturbance rejection control: Methodology, theoretical analysis and applications. In Proceedings of the 29th Chinese control Conference, Beijing, China, 29–31 July 2010; pp. 6083–6090.
24. Jinke, Y.; Hongfei, S. Tracking control for air-breathing hypersonic vehicles based on active disturbance rejection control technique. In Proceedings of the The 26th Chinese Control and Decision Conference (2014 CCDC), Changsha, China, 31 May–2 June 2014; pp. 944–949.
25. Guo, Y.N.; Zhang, X.; Gong, D.W.; Zhang, Z.; Yang, J.J. Novel interactive preference-based multiobjective evolutionary optimization for bolt supporting networks. *IEEE Trans. Evol. Comput.* **2019**, *24*, 750–764. [\[CrossRef\]](#)

26. Xue, J.; Zhuang, K.; Zhao, T.; Zhang, M.; Qiao, Z.; Cui, S.; Gao, Y. Speed Tracking Control of High-Speed Train Based on Particle Swarm Optimization and Adaptive Linear Active Disturbance Rejection Control. *Appl. Sci.* **2022**, *12*, 10558. [[CrossRef](#)]
27. Song, X.F.; Zhang, Y.; Guo, Y.N.; Sun, X.Y.; Wang, Y.L. Variable-size cooperative coevolutionary particle swarm optimization for feature selection on high-dimensional data. *IEEE Trans. Evol. Comput.* **2020**, *24*, 882–895. [[CrossRef](#)]
28. Wang, Z.; Zhao, T. Based on robust sliding mode and linear active disturbance rejection control for attitude of quadrotor load UAV. *Nonlinear Dyn.* **2022**, *108*, 3485–3503. [[CrossRef](#)]
29. Yang, X.; Huang, Q.; Jing, S.; Zhang, M.; Zuo, Z.; Wang, S. Servo system control of satcom on the move based on improved ADRC controller. *Energy Rep.* **2022**, *8*, 1062–1070. [[CrossRef](#)]
30. Vahidi-Moghaddam, A.; Rajaei, A.; Ayati, M.; Vatankhah, R.; Hairi-Yazdi, M.R. Adaptive prescribed-time disturbance observer using nonsingular terminal sliding mode control: Extended Kalman filter and particle swarm optimization. *IET Control. Theory Appl.* **2020**, *14*, 3301–3311. [[CrossRef](#)]
31. Shi, S.; Zeng, Z.; Zhao, C.; Guo, L.; Chen, P. Improved Active Disturbance Rejection Control (ADRC) with Extended State Filters. *Energies* **2022**, *15*, 5799. [[CrossRef](#)]
32. Li, J.; Qi, X.; Xia, Y.; Gao, Z. On asymptotic stability for nonlinear ADRC based control system with application to the ball-beam problem. In Proceedings of the 2016 American Control Conference (ACC), Boston, MA, USA, 6–8 July 2016; pp. 4725–4730.
33. Xu, H.; Mirmirani, M.D.; Ioannou, P.A. Adaptive sliding mode control design for a hypersonic flight vehicle. *J. Guid. Control. Dyn.* **2004**, *27*, 829–838. [[CrossRef](#)]
34. Vaidyanathan, S.; Azar, A.T. An introduction to backstepping control. In *Backstepping Control of Nonlinear Dynamical Systems*; Academic Press: New York, NY, USA, 2021; pp. 1–32.

Disclaimer/Publisher’s Note: The statements, opinions and data contained in all publications are solely those of the individual author(s) and contributor(s) and not of MDPI and/or the editor(s). MDPI and/or the editor(s) disclaim responsibility for any injury to people or property resulting from any ideas, methods, instructions or products referred to in the content.